

Cycle-based signal monitoring using a directionally variant multivariate control chart system

SHIYU ZHOU^{1,*}, NONG JIN¹ and JIONGHUA (JUDY) JIN²

¹*Department of Industrial and Systems Engineering, University of Wisconsin, Madison, WI 53706, USA*
E-mail: szhou@engr.wisc.edu

²*Department of Systems & Industrial Engineering, The University of Arizona, Tucson, AZ 85721-0020, USA*

Received June 2004 and accepted August 2004

Cycle-based signals are generally obtained through the automatic sensing of critical process variables during each repetitive operation cycle of a manufacturing process, and they thus contain a significant amount of information about the process condition. Increasing attention has been paid recently to the problem of effectively monitoring these signals as an aid to the detection of process changes. In general, either based on process engineering knowledge or on historical data analysis, it is possible to obtain process faults and the corresponding signal patterns (the direction and magnitude of a mean shift). In order to fully utilize such fault pattern information in process monitoring, this paper proposes a directionally variant control chart obtained through the effective combination of a multivariate χ^2 chart and a univariate projection chart. It is shown that the addition of the univariate projection chart can improve the detection power for pre-known process faults, however, this may be at the cost of a deterioration in the detection power for unknown faults. A detailed quantitative analysis is provided to justify the application conditions of the proposed chart. A case study of cycle-based tonnage monitoring of a forging process is presented to illustrate the design procedures and the effectiveness of the proposed control chart system.

1. Introduction

The rapid developments obtained in sensing and computer technologies in recent years has allowed the implementation of online measurement of process variables for manufacturing process monitoring and control. *Cycle-based* signals are a very important class of signals observed in many manufacturing processes. As the name implies, a cycle-based signal is a signal obtained using automatic sensing during each repetitive operation cycle of a manufacturing process. For example, tonnage signals (forming force) are measured by the strain gauge sensors installed on a forging press machine. Figure 1(a) illustrates the tonnage signals of two consecutive production cycles that are sampled with respect to the crank angle of a forming press. The vertical axis is the forming force measured in tons, and the horizontal axis is the crank angle of the press. Each cycle-based signal contains 224 data points. In Fig. 1(b), these two cycle-based tonnage signals are aligned as a function of the press crank angle. The similarity of these two signals reflects inherent process characteristics under a given specific operational condition, whereas the differences reflect natural random characteristics due to inevitable process noises. Therefore,

under the same operational conditions, the signals can be assumed to follow an identically independent multivariate distribution, that is, one cycle-based signal is considered to be a single observation of a multivariate random vector. In this paper, the process condition is monitored through detecting the multivariate mean change of the cycle-based signals. Cycle-based signals exist in many manufacturing processes, other than in forging processes, and examples include the forming force in a stamping process, the holding force and current signals in a spot welding process and also the insertion force in an engine assembly process.

Due to the complexity of analyzing high-dimensional cycle-based signals, most industrial practice only uses simple statistics to characterize the cycle-based signals during process monitoring. For example, the maxima magnitude and the average value of the waveform signal are the most commonly used statistics (Knussmann and Rose, 1993). In these methods, a large amount of the process information contained in the signal waveform is not fully utilized. Therefore, a monitoring system based on these simple statistics often suffers from a high false-alarm rate or misdetection rate under changing process conditions.

Recently, process fault diagnosis using cycle-based signals has received a considerable amount of attention from the research community. Several effective techniques have

*Corresponding author

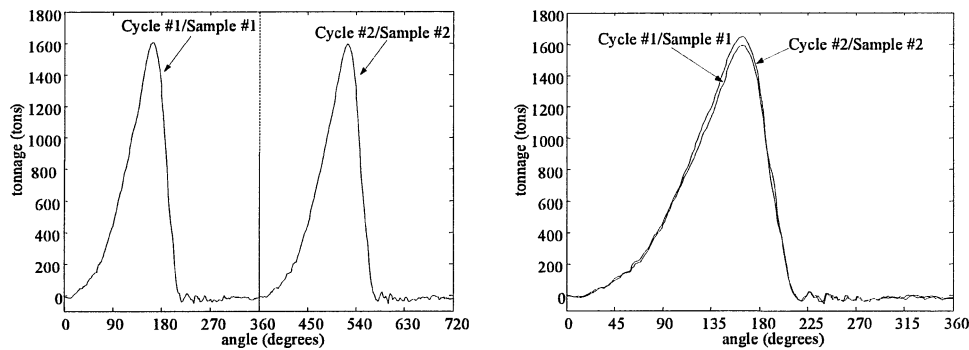


Fig. 1. (a) The forging tonnages of two cycles; and (b) aligned tonnages of two cycles.

been developed that utilize the classification of extracted features of the cycle-based signals, including wavelet-transformation-based methods (Koh *et al.*, 1999a, 1999b; Pittner and Kamarthi, 1999; Jin and Shi, 2001; Lada *et al.*, 2002; Zhou *et al.*, 2003), Principal Component Analysis (PCA) method (Zhou and Jin, 2003) and the Design of Experiments (DOE) method (Jin and Shi, 2000). These techniques focus on automatic clustering and the learning of fault patterns from historical data. As a result, knowledge on process faults and the corresponding signal patterns (e.g., directions and magnitudes of the mean shifts) are continuously accumulated. The objective of this paper is to investigate if the detection power of the monitoring system can be improved by utilizing knowledge about process faults, which are generally ignored in the existing process monitoring techniques.

The available multivariate statistical process monitoring techniques can be roughly categorized into two groups (Pignatiello and Runger, 1990): (i) directionally invariant; and (ii) directionally variant. The directionally invariant multivariate control charts (e.g., the χ^2 control chart and the Hotelling T^2 chart) have equal detection powers regardless of the direction of the mean shift. The directionally invariant chart is “generic” in the sense that there is no assumptions/constraints on the direction of the mean-shift of a potential process fault. Clearly, information on the specific mean-shift direction of known process faults cannot be considered in directionally invariant control charts.

A directionally variant chart detects the mean-shift in a particular direction. Several types of directionally variant charts have been proposed. Healy (1987) proposed a multivariate CUSUM chart that cumulatively sums in a given specific direction. Therefore, the proposed chart is only sensitive to that particular direction. Woodall and Ncube (1985) use simultaneous multiple univariate CUSUM charts to monitor a multivariate process. This chart will be sensitive to the process change in the directions of the respective axes of the process variables. Similarly, Hayter and Tsui (1994) proposed multiple univariate charts to monitor multivariate process variables. Their in-control region is a cube instead of an ellipsoid as in the T^2 chart. They found that in a multivariate setting, neither chart is uniformly

more powerful than the other if the direction of the mean-shift is unknown. Multivariate monitoring based on PCA (Jackson, 1991) is also widely used for the process monitoring of particular directions with large variations. Runger and Montgomery (1997) studied the directional sensitivity and quantified its effect for simultaneous univariate control charts of multivariate process variables. Recently, Runger (1996) proposed a U^2 chart that is based on a projection of all the characteristic variables into a given subspace according to the mean-shift directions of known process faults. If the subspace dimension of the projected variables in the U^2 chart is smaller than the dimension of the original variables, the U^2 chart will in general have a better detection power. However, in the projected subspace, the U^2 chart is constructed using a conventional T^2 chart. Therefore, given two different groups of process faults, the U^2 charts will be identical if the mean-shift directions of those fault groups span the same subspace. Therefore, information on known process faults such as the occurrence probability, the specific mean-shift direction and magnitude is not fully utilized.

The process faults can be generally classified into two categories depending on the available knowledge: one category contains so-called “known faults”, i.e., its multivariate mean-shift direction and magnitude and the occurrence probability are known; and the other category contains so-called “unknown faults”, i.e., the corresponding knowledge of these faults is unknown. A most common situation in practice is that the process has both pre-known faults and unknown faults. The above literature review shows that currently existing directionally variant control charts are mainly designed so as to improve the detection power for known faults with little consideration of the detection power for unknown faults. In this paper, we propose a directionally variant multivariate control chart system that has an improved overall detection power to detect all potential process faults including both known and unknown faults. The basic principle is that in addition to using a directionally invariant control chart to detect all unknown faults, a set of simultaneous univariate control charts are also used to enhance the detection power for potential known faults. It is shown that adding univariate projection charts can

improve the detection power for known faults, however, this may be at the cost of deteriorating the detection power for unknown faults. Thus, the proposed strategy intends to achieve a better overall detection performance by balancing the detection power for both known and unknown faults.

This paper is organized as follows. In Section 2, the principle of the proposed directionally variant multivariate control chart will be presented. The procedures for the control chart design and the performance analysis are also provided. Section 3 presents its application to the cycle-based tonnage monitoring of forging processes to illustrate its effectiveness. The conclusions are presented in Section 4.

2. The proposed directionally variant multivariate control chart

2.1. Problem statement

In this paper, we will consider three types of process conditions: (i) normal working conditions; (ii) known faulty working conditions; and (iii) unknown faulty working conditions. If the i th sample of a cycle-based signal (without causing confusion, a cycle-based signal can here also refer to a cycle-based signal after dimension reduction) is denoted as a p -dimensional random vector \mathbf{x}_i , $\mathbf{x}_i \in \Re^{p \times 1}$. The probability distributions of the cycle-based signal under normal working conditions, known faulty working conditions, and unknown faulty working conditions are denoted as F_0 , $F_j (j = 1, \dots, k)$, and F_{k+1} , respectively. Note that we assume there are k known faulty working conditions. The following assumptions are made on the distributions of \mathbf{x}_i corresponding to each condition.

Assumption 1. when $\mathbf{x}_i \sim F_0$, \mathbf{x}_i is i.i.d. normally distributed with $\mathbf{x}_i \sim N(0, \Sigma)$;

Assumption 2. when $\mathbf{x}_i \sim F_j (j = 1, \dots, k)$, \mathbf{x}_i is i.i.d. normally distributed with $\mathbf{x}_i \sim N(\boldsymbol{\mu}_j, \Sigma)$, $\boldsymbol{\mu}_j$ is nonzero and known. Furthermore, the probability that \mathbf{x}_i follows F_j given that the process is in faulty condition is p_j .

Assumption 3. when $\mathbf{x}_i \sim F_{k+1}$, \mathbf{x}_i is i.i.d. normally distributed with $\mathbf{x}_i \sim N(\boldsymbol{\mu}_u, \Sigma)$ and $\boldsymbol{\mu}_u$ is unknown. However, we assume that the minimal Mahalanobis distance between $\boldsymbol{\mu}_u$ and $\mathbf{0}$ is d_u for all interested unknown faults. Furthermore, the total probability of $\mathbf{x}_i \sim F_{k+1}$ under all unknown faulty working conditions given that the process is in faulty condition is $p_u = (1 - \sum_{j=1}^k p_j)$.

Remark 1. Because we focus on the mean-shift detection in this paper, the covariances matrices of \mathbf{x}_i are assumed to be the same for different working conditions. The mean-shift detection in cycle-based signal monitoring has considerable engineering relevance. For example, the shape changes (mean change) in the tonnage signal can be directly linked to changes in the process setup condition in stamping. However, the covariance of the tonnage signals is determined by interactions between random disturbances in a process.

In most cases, those changes are small and can be ignored. Therefore, the assumption of the same covariance matrix will not severely limit the applications of the proposed method.

Remark 2. We assumed that knowledge of the mean-shift directions under certain process faulty working conditions is known. This information can be obtained through the analysis of DOE data or historical data.

Remark 3. However, it is unreasonable to assume that all the process faulty conditions are known. To simplify the problem, we use a multivariate normal distribution to represent all other unknown faults which have a minimal mean-shift justified by the minimum Mahalanobis distance we want to detect.

The conventional multivariate control charts such as the χ^2 control chart or the available directionally variant charts do not take the information listed in assumptions 2 and 3 into consideration. The objective of this paper is to design a directionally variant control chart that fully utilizes the available information to increase the detection power under the same false-alarm rate compared with conventional charts. Although we use the χ^2 control chart in Phase II monitoring as a comparison benchmark, other similar comparisons can be done for other charts (e.g., the T^2 chart).

The problem of control chart design under assumptions 1–3 can be further formulated as follows. For a multivariate control chart with an in-control region \mathbf{C} (i.e., if $\mathbf{x}_i \in \mathbf{C}$, then \mathbf{x}_i is called “in-control”), the false-alarm rate, also called the Type I error probability, is given as:

$$\alpha = 1 - \int_{\mathbf{x} \in \mathbf{C}} \frac{1}{(2\pi)^{p/2} |\Sigma|^{1/2}} \exp\left(-\frac{1}{2} \mathbf{x}^T \Sigma^{-1} \mathbf{x}\right) d\mathbf{x}, \tag{1}$$

and it is straightforward to obtain that the misdetection rate, also called the Type II error probability, is:

$$\begin{aligned} \beta = & p_u \cdot E_{\boldsymbol{\mu}} \left[\int_{\mathbf{x} \in \mathbf{C}} \frac{1}{(2\pi)^{p/2} |\Sigma|^{1/2}} \right. \\ & \times \exp\left(-\frac{1}{2} (\mathbf{x} - \boldsymbol{\mu}_u)^T \Sigma^{-1} (\mathbf{x} - \boldsymbol{\mu}_u)\right) d\mathbf{x} \Big] \\ & + \sum_{i=1}^k p_i \int_{\mathbf{x} \in \mathbf{C}} \frac{1}{(2\pi)^{p/2} |\Sigma|^{1/2}} \\ & \times \exp\left(-\frac{1}{2} (\mathbf{x} - \boldsymbol{\mu}_i)^T \Sigma^{-1} (\mathbf{x} - \boldsymbol{\mu}_i)\right) d\mathbf{x}. \end{aligned} \tag{2}$$

The first term of Equation (2) is the Type II error caused by the unknown process faults, where $E_{\boldsymbol{\mu}}[\cdot]$ is the expectation with respect to $\boldsymbol{\mu}_u$.

It is known that if $\mathbf{x} \sim N(\boldsymbol{\mu}, \Sigma)$, then $\mathbf{y} \sim N(\Sigma^{-1/2} \boldsymbol{\mu}, \mathbf{I})$, where $\mathbf{y} = \Sigma^{-1/2} \mathbf{x}$ and \mathbf{I} is an identity matrix. Therefore, without loss of generality, it can be assumed that the covariance matrices under consideration are all identity matrices

to simplify the derivation. Hence, the expression of Σ in Equations (1) and (2) can be replaced by \mathbf{I} .

Consideration of Equations (1) and (2) leads us to believe that actually the control chart design can be formulated as an optimization problem of the form of:

$$\beta^* = \min_C[\beta], \text{ subject to } \alpha = \text{constant.} \quad (3)$$

In other words, we want to find the control limits or the in-control region \mathbf{C} to minimize Type II error under the constraint of a given Type I error. Without causing confusion, we use the same symbol \mathbf{C} for the control limits.

It is in general very difficult to obtain the global optimal solution of the problem in Equation (3). In this paper, we present a suboptimal solution to this problem, which ensures that we are able to provide a higher detection power than a conventional multivariate control chart.

2.2. The principles behind the proposed directionally variant multivariate control chart

The proposed directionally variant multivariate control chart consists of two sets of control charts:

1. a χ^2 control chart, denoted as the χ_{DV}^2 chart; and
2. k simultaneous univariate charts for $y_{ji}, j = 1 \dots k$, where $y_{ji} = \mathbf{v}_j^T \mathbf{x}_i$ and \mathbf{v}_j is the direction vector of the mean shift of F_j , i.e., $\mathbf{v}_j = \boldsymbol{\mu}_j / |\boldsymbol{\mu}_j|$. These univariate charts are denoted as the $u_j^{\text{DV}} (j = 1 \dots k)$ chart.

For the combination of the χ_{DV}^2 chart and the $u_j^{\text{DV}} (j = 1 \dots k)$ charts, the joint decision rule is that the system is out of control when any one of the control charts indicates an out-of-control condition. Based on this rule, the control limits of the proposed control chart can be obtained as in Fig. 2.

In Fig. 2, the solid circle with radius r_1 is the control limit of the χ_{DV}^2 chart. The lines that are perpendicular to the mean vectors ($\boldsymbol{\mu}_1$ and $\boldsymbol{\mu}_2$) of known faulty conditions are the control limits with c_1 and c_2 in the u_j^{DV} charts ($j = 1, 2$). The intersection of the in-control regions of these three control charts is represented by the bold solid line, within

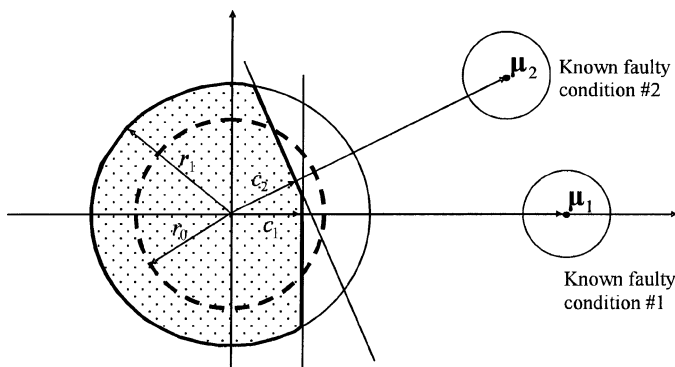


Fig. 2. Illustration of the proposed control charts.

which is the in-control region denoted as \mathbf{C}_{DV} of the combined control chart system. Clearly, the proposed chart is a directionally variant chart having different detection powers for the two known faults and the unknown faults. To design this control chart, we need to specify the parameters r_1 and $c_j, j = 1 \dots k$.

For comparison, the control limit of a conventional χ^2 control chart (denoted as χ_c^2) is also illustrated in the figure as the dashed-line circle with the radius of r_0 . The in-control region of the χ_c^2 chart is denoted as \mathbf{C}_c . To design this control chart, we only need to specify the parameter r_0 . We say that the proposed control chart is a better control chart than the conventional χ_c^2 chart if: (i) $P(\mathbf{x}_i \in \mathbf{C}_{\text{DV}}) = P(\mathbf{x}_i \in \mathbf{C}_c)$ when $\mathbf{x}_i \sim F_0$; and (ii) $P(\mathbf{x}_i \in \mathbf{C}_{\text{DV}}) < P(\mathbf{x}_i \in \mathbf{C}_c)$ when $\mathbf{x}_i \sim F_j$, for some $j \in \{1, \dots, k + 1\}$ where $P(A)$ is the probability of event A .

2.3. Conditions for detection power increase using the directionally variant control chart

Before we go into the design steps of finding the parameters r_1 and $c_j, j = 1 \dots k$, we need to first answer the question of “under what conditions is the proposed control chart better than a conventional multivariate control chart?” To provide a better understanding of the problem, we investigate the simplest case of one known faulty condition.

In this case, the proposed control chart consists of one χ_{DV}^2 chart and one u_1^{DV} chart. The χ_{DV}^2 chart aims to detect the existence of F_2 , and the u_1^{DV} chart aims to detect the existence of F_1 . It is expected that the u_1^{DV} chart is more sensitive than the χ_{DV}^2 chart in detecting the known fault F_1 . This is confirmed by the following proposition.

Proposition 1. *Given a directionally variant chart (combining χ_{DV}^2 and u_1^{DV} as illustrated in Fig. 3) with the control limits of r and c , respectively, then, the Type II error probability for the detection of the known fault F_1 (denoted as β_1) is monotonically decreasing with respect to r if the Type I error probability of the directionally variant chart is fixed as α , i.e., $d\beta_1/dr < 0$ if α is a constant.*

Proof. The detailed proof of this proposition is listed in the Appendix. ■

The result can be interpreted using Fig. 3.

The shaded region in Fig. 3 is \mathbf{C}_{DV} . When the control limit of the u_1^{DV} chart is moved close to the origin (i.e., c decreases), the control limit of the $\chi_{\text{DV}}^2 (r^2)$ should increase to keep a constant total Type I error probability. Clearly, the detection power of the known fault ($1 - \beta_1$) will increase when c decreases and conversely it will decrease when r increases. The result of Proposition 1 indicates that the gain in detection power is more significant than the loss and hence $1 - \beta_1$ will increase when α is kept constant and c decreases. Furthermore, it can be seen that the detection power of a combined chart is larger than that of a conventional χ_c^2 chart for the known process fault condition

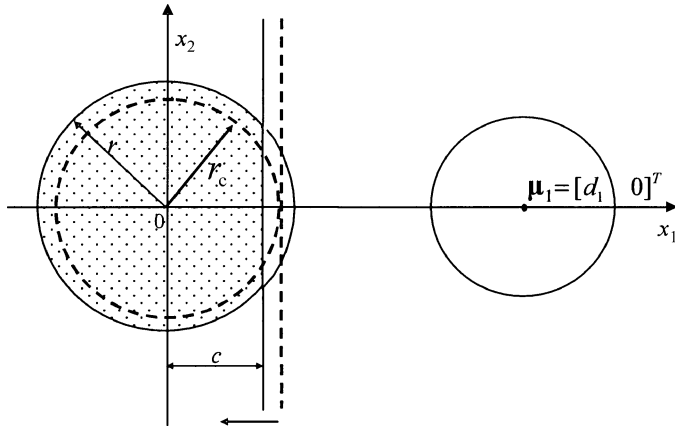


Fig. 3. The χ_{DV}^2 chart and the u_1^{DV} chart with one known fault.

when $c < r_c$. The detection power of the combined chart for the unknown fault F_{k+1} is not necessarily higher than the conventional χ_c^2 chart. This is shown in Fig. 4.

As an example, for a two-dimensional case, the combined control charts are set up as in Fig. 3 and the total Type I error of the two charts is $\alpha = 0.05$. The radius of a conventional χ_c^2 chart with the same Type I error of $\alpha = 0.05$ is 2.43. We assume that the mean locations of all interested unknown faults of F_2 are evenly distributed on a circle with a radius of five. For the combined charts, the Type II error probability is calculated based on Equation (2) ($p_u = 1$ in this case) using a numerical integration method. The resulting Type II error probability of the u_1^{DV} chart, χ_{DV}^2 chart, and the combined charts are plotted versus r . Clearly, when r gets larger, the probability of misdetection of unknown faults increases and it is larger than that of a conventional χ_c^2 chart. Another

interesting point that can be seen from Fig. 4 is that the unknown fault is mainly detected by the χ_{DV}^2 chart in the combined chart: the probability of misdetection by the u_1^{DV} chart for unknown faults is quite high (above 0.6) and the curve of the combined chart is quite close to the curve of the χ_{DV}^2 chart. This analysis can be further summarized as the following two remarks:

Remark 4. Only using a directionally variant chart could result in a large probability for misdetection of the unknown faults. To guarantee the overall detection power, combining both directionally variant and directionally invariant charts is a better strategy. This is the major difference between the proposed method and the currently available directionally variant charts.

Remark 5. Because the directionally variant chart (u_1^{DV} chart in Fig. 3) plays a less important role in detection of the unknown faults, we can use the probability of misdetection by the χ_{DV}^2 chart to approximate the probability of misdetection of the combined chart for unknown faults. Obviously, the approximated value will always be larger than the actual value because the condition of $P\{\mathbf{x}_i \in \chi_{DV}^2 \mid F_2\} \cap [\mathbf{x}_i \in u_1^{DV} \mid F_2] \leq P\{\mathbf{x}_i \in \chi_{DV}^2 \mid F_2\}$ always holds.

The proposed combined control chart has an improved detection power for the known process fault but a deteriorated detection power for the unknown process fault. For a process with both known and unknown process faulty conditions, which is the most common situation in practice, the detection power of the proposed combined chart is a trade-off between these two factors. Since there is no closed-form expression available for the integral result of the normal density function on an irregular area C_{DV} , a numerical integral calculation is used to investigate the criteria for which the combined control charts have a better detection power than the conventional χ_c^2 chart.

The basic steps of the numerical method of finding the criteria are illustrated below using a single known fault case. The general design procedure of the combined control chart system is presented in Section 2.4.

The total Type II error of the combined chart is affected by the specified Type I error and its allocation of the Type I error (α_0) in the χ_{DV}^2 control chart and Type I error (α_1) in the u_1^{DV} . Figure 5(a) shows the relationship between α_0 and α_1 for a given fixed overall Type I error $\alpha = 0.05$. An optimization problem of:

$$\min_{\alpha_1} [|\alpha - f(\alpha_0, \alpha_1)|],$$

is solved to obtain Fig. 5(a), where $f(\alpha_0, \alpha_1)$ is the overall Type I error based on Equation (1). To evaluate Equation (1), we need to calculate the integral of a multivariate normal distribution on an irregular region C_{DV} (e.g., the shaded area in Fig. 2). The Monte Carlo simulation method (Press *et al.*, 1993) is used in this paper because it is good at the integral calculation of a smooth function on extremely

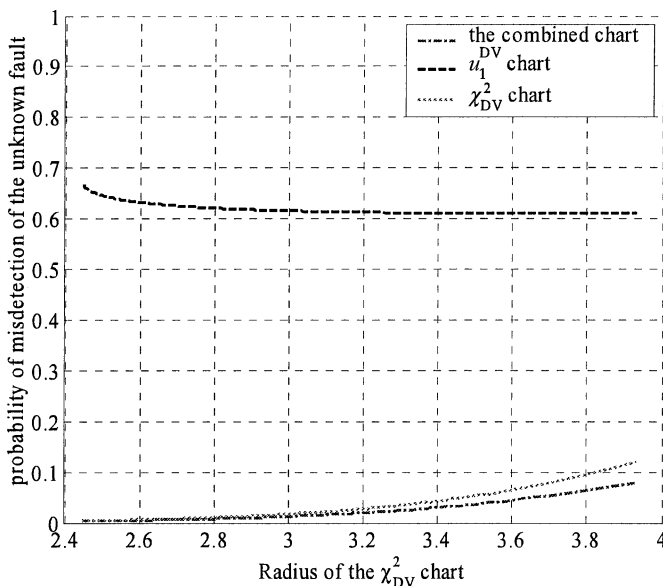


Fig. 4. The probability of misdetection of the unknown faults.

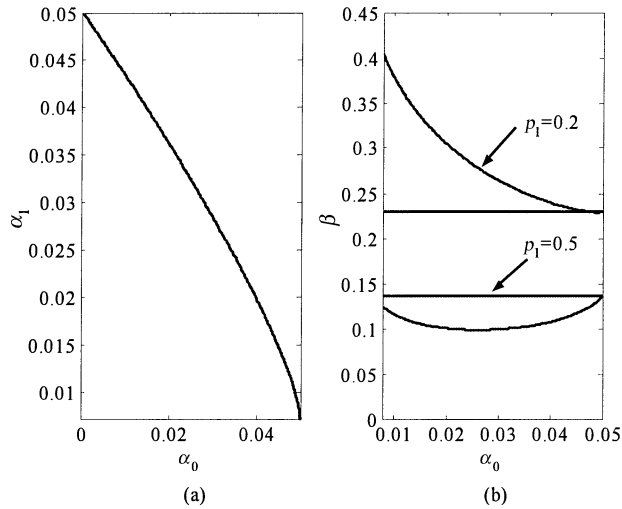


Fig. 5. (a) The relationship between α_1 and α_2 for a fixed overall Type 1 error when $\alpha = 0.05$; and (b) the Type II error of the combined chart.

irregular areas. Due to the smoothness of the cost function $|\alpha - f(\alpha_0, \alpha_1)|$, the optimization can be simply done using a binary search or golden section search method (Press *et al.*, 1993).

Figure 5(b) shows the Type II error of the combined chart as a function of α_0 when $p_1 = 0.2$ and 0.5 . Here, the mean shifts of F_1 and F_2 are defined as d_1 and d_u , respectively, and both of them are set equal to three. Equation (2) can be used to calculate the total Type II error of the combined chart. As discussed above, the first term of the right-hand

expression of Equation (2) can be approximated by solely using the Type II error probability of the χ_{DV}^2 chart. The Type II error probability of a conventional χ_c^2 chart given the same fixed $\alpha = 0.05$ is also shown as two horizontal lines in Fig. 5(b). One significant characteristic of Fig. 5(b) is that the Type II error probability of the combined chart is not always smaller than that of a conventional χ_c^2 chart. It depends on the design of the combined control chart and the behavior of the known faults. When the unknown fault F_2 dominates as at the conditions of $d_1 = 3, d_u = 3, p_1 = 0.2$, it is possible that no matter how we select the χ_{DV}^2 chart and the u_1^{DV} chart, we cannot achieve a better detection power to that of a conventional χ_c^2 chart.

An operation-characteristic curve as shown in Fig. 6 (a–d) is developed to determine the sufficient condition of obtaining benefits by using the combined chart when one known fault exists. Figure 6 (a–d) provides the selection criteria for the combined chart under several typical situations. We denote $\beta_c(d_1, d_u, p_1, \alpha)$ as the Type II error of the conventional χ_c^2 chart, $\beta_{DV}(d_1, d_u, p_1, \alpha_0, \alpha)$ as the Type II error of the combined chart, where α_0 is the Type I error of the χ_{DV}^2 chart, and the increase in the detection power by using the combined chart is denoted by γ_{gain} where $\gamma_{\text{gain}} = \beta_c(d_1, d_u, p_1, \alpha) - \beta_{DV}(d_1, d_u, p_1, \alpha_0, \alpha)$. The curve is the smallest d_u such that for a given α error, d_1 , and p_1 , the γ_{gain} of using the combined chart is 0.001. In general, an increase in d_u will reduce the contribution of the unknown faults to the overall Type II error. Therefore, for a given condition of α, d_1, p_1 , and d_u , if the point (d_1, d_u) falls above the designated curve, we can reduce the overall Type II error by at least 0.001 using the combined control chart. Therefore,

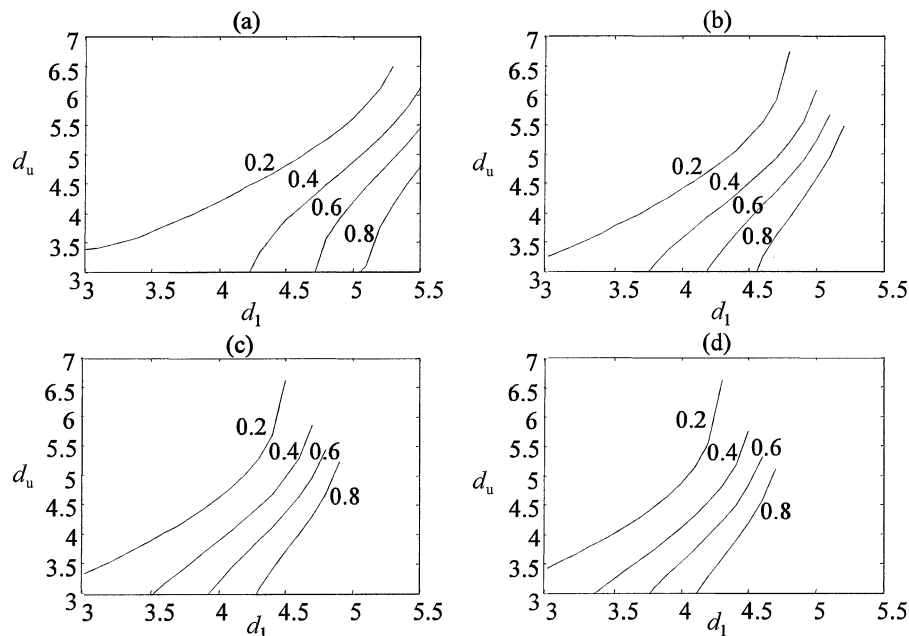


Fig. 6. The criteria of adopting the combined chart ($p_1 = 0.2, 0.4, 0.6$, and 0.8 , respectively): (a) $\alpha = 0.01$; (b) $\alpha = 0.05$; (c) $\alpha = 0.10$; and (d) $\alpha = 0.15$.

Fig. 6 (a–d) can be used to check if the detection power will be increased using the proposed combined control charts.

In Fig. 6 (a–d) we assume that $d_1 \geq 3$ and $d_u \geq 3$. The rationale is that when the mean shifts of the process faults are too small, it is impossible to design a control chart that has both an acceptable small Type I error and Type II error. Although we can still increase the detection power by using the combined charts as compared to the conventional method, the total β error is too large to be accepted when the mean shifts are small. The curves in Fig. 6 (a–d) clearly show that the overall detection power increase of the combined chart is mainly contributed by the detection power increase of the known process fault: when the weight of the known fault increases from 0.2 to 0.8, the curve moves from left to right.

2.4. Design procedure of the directionally variant control chart

The discussion of the single known fault case provides the intuitive understanding of the design principles of the proposed combined control chart. If there are k known faults in the system, k projection charts $u_j^{DV}, j = 1 \dots k$, need to be used. Inevitably, the justification and design of the combined control chart is more complicated. If there are k known faults, we need to select $k + 1$ parameters (k parameters for the $u_j^{DV}, j = 1 \dots k$, charts and one for the χ_{DV}^2 chart). These parameters are designed under the constraint of the overall Type I error. To simplify the problem and provide generic guidelines on the design of a combined control chart for multiple known process faults, we first adopt a “conservative” rule: the control limits of all the $u_j^{DV}, j = 1 \dots k$, charts are the same. This rule reduces the design parameters from $k + 1$ to two. Clearly, if we can increase the detection power using the combined chart under this rule, we can certainly further improve the performance of the control charts by allowing different control limits for the $u_j^{DV}, j = 1 \dots k$, charts.

Similar to the single known fault case, the use of the combined chart is not always beneficial in terms of the overall detection power. We will provide some generic conditions and justification of the use of the proposed combined charts.

First, the Type II error of detecting all known process faults (β_p) can be obtained as:

$$\beta_p = \sum_{j=1}^k p_j \beta_j(\alpha_p, \alpha_0, d_j). \quad (4)$$

In Equation (4), β_j is the Type II error in detection of F_j . The numbers d_j and p_j are the distance of the mean-shift and the probability of the occurrence of F_j , respectively. α_p and α_0 are the Type I error probabilities of the $u_j^{DV}, j = 1 \dots, k$, charts and the χ_{DV}^2 chart, respectively. It should be noted that α_p and α_0 are not independent because they need to satisfy the requirement of the overall α error. Similarly, the Type II error of the conventional χ_c^2 chart in detecting all

known process faults β_{pc} can be obtained as:

$$\beta_{pc}^1 = \sum_{j=1}^k p_j \beta_{jc}(\alpha, d_j), \quad (5)$$

where β_{jc} is the Type II error of detecting F_j in the conventional χ_c^2 chart. In most cases, β_{pc} larger than β_p .

On the other hand, the Type II error of the combined chart for the detection of the unknown fault (F_{k+1}) generally increases. Denote by β_u and β_{uc} the Type II error of the combined charts and the conventional χ_c^2 chart for detection of F_{k+1} , respectively. The loss in detection power by using the combined charts can be obtained as $\gamma_{loss} = p_u(\beta_u - \beta_{uc})$, where p_u is the probability of the occurrence of F_{k+1} . Similar to the case of a single known fault, we approximate the γ_{loss} as the difference between the Type II errors of the conventional χ_c^2 chart and the χ_{DV}^2 chart. Using this approximation, the β_u is only a function of α_0 of the χ_{DV}^2 and the mean-shift distance of the unknown fault d_u .

It is clear that if $(\beta_{pc} - \beta_p)$ is larger than $p_u(\beta_u - \beta_{uc})$, i.e., if:

$$(\beta_{pc} - \beta) + p_u(\beta_{uc})/p_u > \beta_u, \quad (6)$$

then the combined control charts have more detection power than the conventional χ_c^2 chart. Therefore, we can compare the value of the left-hand side of Equation (6) and β_u to determine if it is beneficial to use the combined chart.

Figure 7 illustrates the relationship between β_u and α_0 for a given d_u (the number marked on the curves). Obviously, β_u will decrease with an increase in α_0 for a fixed d_u or with an increase in d_u for a fixed α_0 . Clearly, Fig. 7 can be used to determine the gain in detection power by using the proposed control charts under different variable dimensions.

An example of utilizing Fig. 7 is shown in Fig. 8. The dimension of the process variable is four and there are three known process faults (F_1, F_2, F_3) with mean-shift locations at $\mu_1 = 3[1 \ 0 \ 0 \ 0]^T$, $\mu_2 = 4[1/\sqrt{2} \ 1/\sqrt{2} \ 0 \ 0]^T$ and $\mu_3 = 4[1/\sqrt{2} \ 0 \ 0 \ 1/\sqrt{2}]^T$, respectively. The probabilities of F_1, F_2 , and F_3 are $p_1 = 0.2, p_2 = 0.3$, and $p_3 = 0.3$ respectively. The mean-shift distance of unknown fault F_4 is set at three. Based on these parameters, we can calculate $(\beta_{pc} - \beta_p + p_u\beta_{uc})/p_u$ with respect to the α_0 for a given overall α . The procedure is as follows:

1. For a given Type I error for the χ_{DV}^2 chart in the combined charts, denoted as α_0 and $0 < \alpha_0 < \alpha$, find the Type I error (α_1) of the projection charts to satisfy the overall Type I error. In this example, the overall α error is set at 0.05.
2. Based on the selected α_0 and α_1 , the Type II error for detecting the known faults are calculated. The computation requires a multi-dimensional normal integral calculation on an irregular area. The Monte Carlo simulation method is used. A large number ($N = 1,000,000$) of four-dimensional normal distributed data points are generated and the number of data points that fall in the

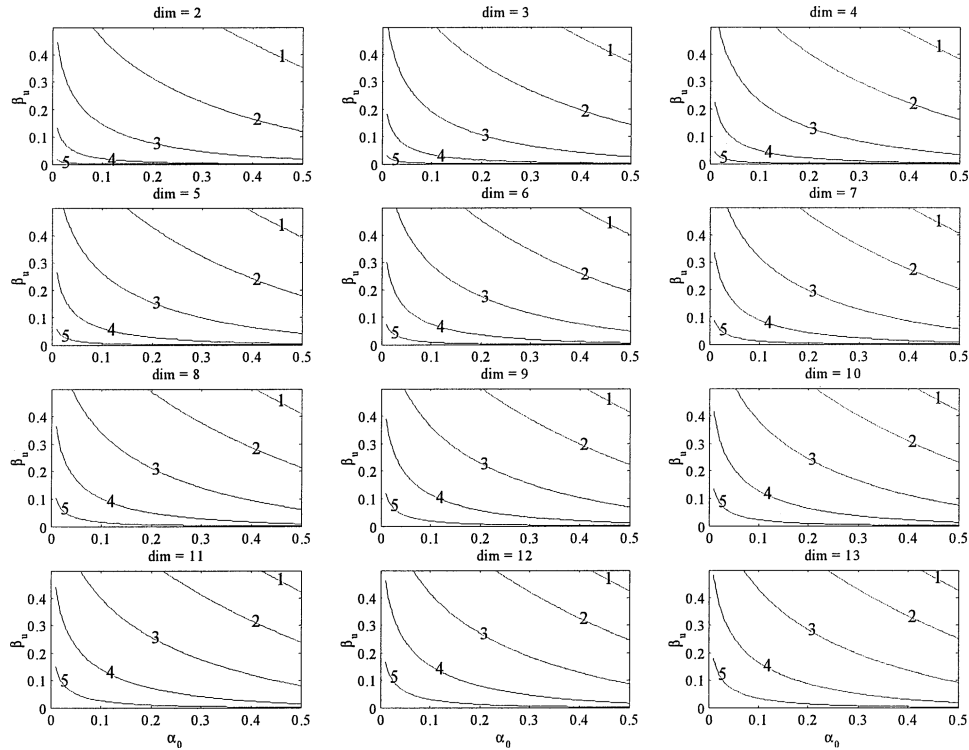


Fig. 7. The relationship between β_u and α_0 for a given d_u .

irregular control limits are counted as n . The in-control probability is taken as n/N . This integral calculation method is also used in Hayter and Tsui (1994).

3. The Type II error of the conventional χ^2_c chart can be calculated using the regular non-central χ^2 distribution. The degree-of-freedom is four and the non-central parameter is the square of the mean-shift distance.

Following the above procedure, the curve of $(\beta_{pc} - \beta_p + p_u\beta_{uc})/p_u$ against α_0 can be generated. If this curve is overlapped with the corresponding contour curve of Fig. 7, we

can easily determine if the combined control charts can be used to reduce the overall Type II error, i.e., if the curve of $(\beta_{pc} - \beta_p + p_u\beta_{uc})/p_u$ is above the corresponding curve (the curve marked “3” in Fig. 8) of β_u , then the overall Type II error can be reduced. Furthermore, by checking the difference between these two curves, we can select a good α_0 value. For example, in Fig. 8, this difference approximately reaches a maximum value at about $\alpha_0 = 0.03$. Therefore, $\alpha_0 = 0.03$ could be used for the combined control charts.

We have discussed the justification for using the proposed combined control charts when some of the process faults are known. A summary of the design procedures is given as follows:

- Step 1. Find the mean-shift locations ($\mu_i, j = 1 \dots k$) of the typical process faults and their occurrence probabilities ($p_i, j = 1 \dots k$) when a process fault occurs. This information can be obtained from an analysis of historical production data.
- Step 2. Define the critical mean-shift distance of the unknown faults. For all unknown faults with a total occurrence probability of $p_u = (1 - \sum_{j=1}^k p_j)$, engineering specification is used to justify the minimum distance of d_u (the critical magnitude of the mean-shift of the unknown faults that we want to detect).
- Step 3. Justify the use of the combined chart. If there is only one known fault ($k = 1$), Fig. 6 (a–d) can be used to check if the detection power can be improved by

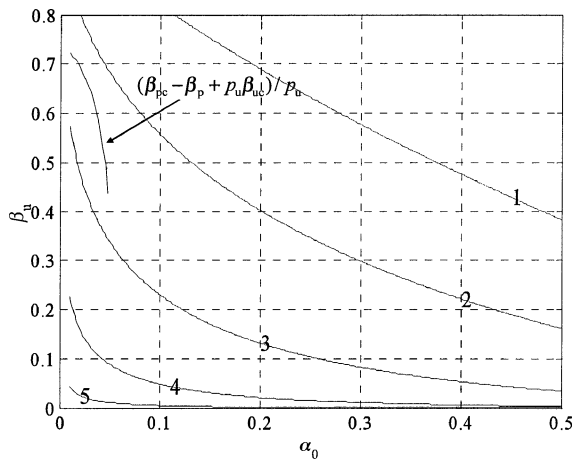


Fig. 8. Justification for using the combined control charts for multiple faults.

using the combined chart. If multiple known faults exist ($k > 1$), then the procedures introduced in this section need to be followed. In more detail,

- The first step is to decide the nonparametric relationship between the Type I error (α_1) of the u_j^{DV} , $j = 1 \dots k$ charts, and the Type I error (α_0) of the χ_{DV}^2 chart under the constraint of a fixed overall Type I error.
- Knowing the nonparametric relationship between α_0 and α_1 for a given fixed α , the curve of $(\beta_{pc} - \beta_p + p_u \beta_{uc})/p_u$ against α_0 can be obtained. Using Fig. 7, we can determine if the detection power of the combined chart is better than the conventional χ_c^2 chart.

Step 4. After the benefit of using the combined chart is confirmed through Step 3, the optimal α_0 and corresponding α_1 can be obtained by reading the curve of the difference between the Type II error probability of the conventional χ_c^2 chart and that of the combined chart (e.g., Fig. 8 for the case of multiple known faults or Fig. 5(b) for the case of a single fault).

After these four steps, the control limits of the χ_{DV}^2 chart and the univariate projection charts can be decided. A practical example using cycle-based tonnage signal monitoring is illustrated in the following section to demonstrate the application of the developed control chart system.

3. Case study: forging process monitoring

The forging operation is an important manufacturing process in which metal is formed, under impact or pressure, to produce a desired shape with improved material properties. A forging process usually begins with stock preparation, cut-off, cleaning, inspection and heating. The key step is the deformation step. This step is done by a forging press. Figure 9 shows a simplified diagram of the structure of a mechanical forging press. In this type of press, the forming energy is provided by the kinetic energy stored in the flywheel.

The forging process is a very complicated manufacturing process. The final product quality can be affected by many factors, e.g., the die conditions, lubrication, perform operation, workpiece properties, temperature, and process setting parameters such as shut height etc. (Arentoft and Wanheim, 1997).

The tonnage as illustrated in Fig. 1 is a very important process variable that reflects the forging press' condition, such as the lubrication, wear conditions, etc. For each cycle of the forging operation, a tonnage signal can be obtained. It is highly desired to develop a methodology to analyze and monitor the cycle-based tonnage signals (Barnett *et al.*,

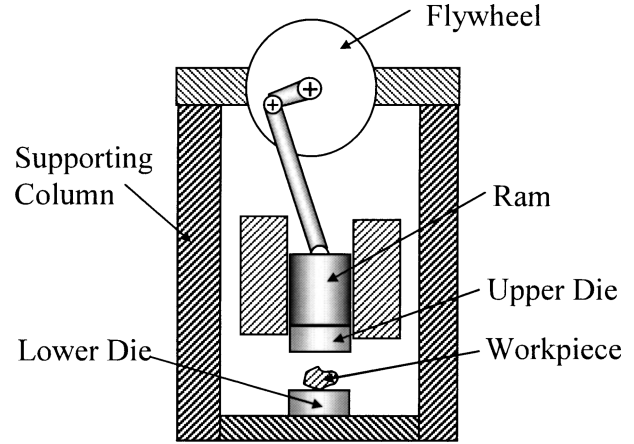


Fig. 9. A diagram of a mechanical forging press.

1998). The proposed control chart system can be used in this case.

Since a tonnage signal is a high-dimensional random vector, a dimension reduction step that can effectively extract the variation patterns from the signal is needed to apply the control chart technique. Using PCA 10 critical features can be extracted from the tonnage signals. Using a historical dataset with 573 samples, several working conditions can be identified from these 10 features: (i) Normal working conditions with a mean of $\mathbf{0}$; (ii) faulty working condition no. 1 with a mean of $\mu_1 = [2.4112 \ -0.4908 \ -0.9129 \ -0.3412 \ 0.2679 \ 0.7083 \ 0.1291 \ -0.1403 \ -0.1460 \ 0.0566]^T$, which contains 105 samples; (iii) faulty working condition no. 2 with a mean of $\mu_2 = [5.5100 \ -0.0673 \ -0.6282 \ -0.1261 \ 0.1454 \ 2.8300 \ 1.0287 \ -0.5130 \ 0.2080 \ -0.4495]$, which contains 39 samples; and (iv) some scattered faulty working conditions with unknown sources, which contains 77 samples with the average distance of 4.0 from zero. Based

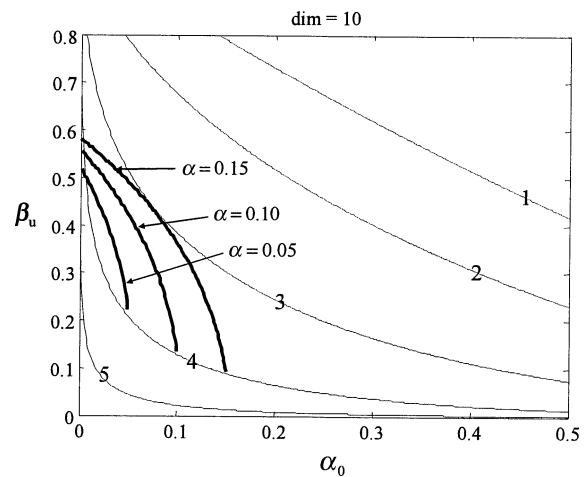


Fig. 10. The β error of the combined charts and the conventional χ_c^2 chart.

Table 1. Comparison between the conventional χ_c^2 chart and the combined charts

Overall α	α_0		β_1		β_2		β_3		β	
	α_0	α_1	χ_c^2	New	χ_c^2	New	χ_c^2	New	χ_c^2	New
0.05	0.0255	0.0200	0.585	0.207	0.002	0.000	0.207	0.293	0.351	0.201
0.1	0.0562	0.0390	0.455	0.131	0.001	0.000	0.128	0.192	0.261	0.129
0.15	0.0881	0.0591	0.369	0.091	0.000	0	0.089	0.142	0.206	0.092

on the number of samples in each working condition, the probability of the occurrence of the fault conditions can be approximately estimated as $p_1 = 47.51\%$, $p_2 = 17.66\%$, and $p_u = 34.83\%$. Using these parameters, the directionally variant control charts can be designed. Following the procedure described in Section 2.4, we can determine if the detection power can be increased by using the combined charts. The results are shown in Fig. 10 for different overall Type I error probabilities (i.e., $\alpha = 0.05$, $\alpha = 0.10$, and $\alpha = 0.15$ respectively).

The bold curves in Fig. 10 are the curves of $(\beta_{pc} - \beta_p + p_u\beta_{uc})/p_u$. If the bold curve is above the corresponding curve (the curve marked with a “4” in this case, which means $d_u = 4.0$) of β_{uc} the detection power can be increased. The figure indicates that benefit can be obtained by using the combined chart in a large range of α_0 . The optimal α_0 can be obtained by further checking the magnitude of the difference. A detailed comparison between the proposed combined chart and the conventional χ_c^2 chart is given in Table 1.

In Table 1, the columns headed by α_0 and α_1 are the optimal values of the Type I errors of the χ_{DV}^2 chart and the projection u_1^{DV} and u_2^{DV} charts, respectively. The columns headed by β_1 , β_2 , and β_3 are the Type II errors of detecting the abnormal working conditions #1, and #2, and the unknown fault by using the conventional χ_c^2 chart and the combined charts, respectively. The last column provides a comparison of the overall Type II errors of the conventional chart and the proposed combined charts. From this result, it can be seen that the proposed combined charts have a significantly higher detection power than the conventional χ_c^2 chart.

4. Conclusions and discussion

In this paper, we have proposed a directionally variant multivariate control chart to monitor cycle-based signals. Unlike either the conventional multivariate control charts such as the χ^2 chart that do not consider the available information about the process faulty conditions or the discrimination analyses that assume that the process faulty conditions are completely known, we classify the process faulty conditions into two categories: (i) the known faulty condition; and (ii) the unknown faulty condition. Our rationale is that in most cases, some process faulty conditions manifested

in the cycle-based signal can be obtained from engineering design, DOE, or abundant historical data.

We have shown that for known process faulty conditions, the detection power of the conventional multivariate control such as χ_c^2 charts is improved by adding simultaneous univariate “projection” control charts. Therefore, a directionally variant control chart was designed by combining both a multivariate χ^2 chart and univariate charts. However, for the unknown faulty condition, the detection power of the combined chart could be reduced. The overall benefits of using the proposed combined control charts are determined by the trade-off between the known faulty condition and the unknown faulty condition. We discussed the generic conditions and justification for using the proposed charts. We have shown that an increase in the known fault occurrence probability or the mean-shift distance of the unknown faults, results in an improvement in the overall detection power of the combined control chart. For the convenience of implementation under a single known fault condition, we provided a set of plots shown in Fig. 6 (a–d) for users to directly check the conditions for the use of the proposed charts. For multiple faults, a set of typical plots of β_u are shown in Fig. 7, which can be used to identify the conditions to use the combined charts under a common range of data dimension ranging from two to 13. A forging tonnage monitoring example was presented to illustrate the effectiveness of this method.

A couple of interesting problems are left open. The first one is the impact of the accuracy of the known and unknown faulty conditions (their mean-shift direction and the occurrence probability) on the performance of the proposed control charts. In most cases, the process working conditions need to be estimated based on historical data. Ultimately, the estimation method and the control chart design need to be considered together to achieve the best detection power. This problem is currently under investigation. The second point is that the developed control chart system consists of a χ^2 chart and some simple univariate projection control charts. However, this should not be the only way to combine different types of control charts together for the effective detection of both known and unknown process faulty conditions. For example, EWMA and CUSUM charts are quite effective in detecting small mean shifts. They can be used as replacements for the Shewhart type of control charts to detect the small mean shifts of known faults. Although the design guidelines might need

to be modified, the basic idea of combining different charts together to improve the performance remains unaltered.

Acknowledgements

The authors gratefully acknowledge the financial support from the NSF under grant DMI-0330356 and DMI-0133942. The authors also thank the editor and referees for their valuable comments and suggestions.

References

Arentoft, M. and Wanheim, T. (1997) The basis for a design support system to prevent defects in forging. *Journal of Materials Processing Technology*, **69**, 227–232.

Barnett, K., Duggirala, R., Hitz, D. and Spiewak, S. (1998) Monitoring and control of equipment and process in cold extrusion. *Journal of Materials and Manufacturing*, 991–1001.

Hayter, A.J. and Tsui K. (1994) Identification and quantification in multivariate quality control problems. *Journal of Quality Technology*, **26**(3), 197–208.

Healy, J.D. (1987) A note on multivariate CUSUM procedures. *Technometrics*, **29**, 409–412.

Jackson, J.E. (1991) *A User's Guide to Principal Components*, Wiley, New York, NY.

Jin J. and Shi J. (2000) Diagnostic feature extraction from stamping tonnage signals based on design of experiments, *ASME Transactions Journal of Manufacturing Science and Engineering*, **122** (2), 360–369.

Jin, J. and Shi, J. (2001) Automatic feature extraction of waveform signals for in-process diagnostic performance improvement. *Journal of Intelligent Manufacturing*, **12**, 257–268.

Johnson, R.A. and Wichern, D.W. (1998) *Applied Multivariate Statistical Analysis*, 4th edn., Prentice Hall, Upper Saddle River, NJ.

Knussmann, K.D. and Rose, C. (1993) Signature-based process control (SbPC™). *Signature Technologies Technical Reports*, pp. 311–325.

Koh, C.K.H., Shi, J., Williams, W. and Ni, J. (1999a) Multiple fault detection and isolation using the Haar transform—part 1: theory. *ASME Transactions Journal of Manufacturing Science and Engineering*, **121**(2), 290–294.

Koh, C.K.H., Shi, J., Williams, W. and Ni, J. (1999b) Multiple fault detection and isolation using the Haar Transform—part 2: application to the stamping process. *ASME Transactions Journal of Manufacturing Science and Engineering*, **121**(2), 295–299.

Lada, E.K., Lu, J.C. and Wilson, J.R. (2002) A wavelet-based procedure for process fault detection. *IEEE Transactions on Semiconductor Manufacturing*, **15**(1), 79–90.

Pignatiello, J. and Runger, G.C. (1990) Comparisons of multivariate CUSUM charts. *Journal of Quality Technology*, **22**(3), 173–186.

Pittner S. and Kamarthi S. V. (1999) Feature extraction from wavelet coefficients for pattern recognition tasks. *IEEE Transactions on Pattern Analysis and Machine Intelligence*, **21**(1), 83–88.

Press, W.H., Flannery, B.P., Teukolsky, S.A. and Vetterling, W.T. (1993) *Numerical Recipes in C: The Art of Scientific Computing*, 2nd edn., Cambridge University Press: Cambridge, UK.

Runger, G.C. (1996) Projection and the U² multivariate control chart. *Journal of Quality Technology*, **28**(3), 313–319.

Runger, G.C. and Montgomery, D.C. (1997) Multivariate and univariate process control: geometry and shift directions. *Quality and Reliability Engineering International*, **13**, 153–158.

Woodall, W.H. and Ncube, M.M. (1985) Multivariate CUSUM quality control procedures. *Technometrics*, **27**(3), 285–292.

Zhou, S. and Jin, J. (2005) An unsupervised clustering method For cycle-based waveform signals in manufacturing processes. *IIE Transactions*, **37**, 569–584.

Zhou, S., Sun, B. and Shi, J. (2005) An SPC monitoring system for cycle-based waveform signals using Haar transform. *IEEE Transactions on Automation Science and Engineering*, (in press).

Appendix

Proof of Proposition 1. Firstly, consider the two-dimensional case. Without loss of generality, we assume that the mean of F_1 is located at $(d_1, 0)$. The control limit of the combined control charts, denoted as C_{DV} , is the contour of the shaded region in Fig. 3. By definition, we have:

$$\int_{C_{DV}} f_0(x_1, x_2)dx_1dx_2=1-\alpha, \quad \int_{C_{DV}} f_1(x_1, x_2)dx_1dx_2=\beta_1, \tag{A1}$$

where

$$f_0(x_1, x_2) = \frac{1}{2\pi} \exp\left(-\frac{1}{2}(x_1^2 + x_2^2)\right) \quad \text{and}$$

$$f_1(x_1, x_2) = \frac{1}{2\pi} \exp\left(-\frac{1}{2}[(x_1 - d_1)^2 + x_2^2]\right),$$

are the probability distribution functions of process measurement $\mathbf{x} = [x_1, x_2]^T$ when $\mathbf{x} \sim F_0$ and $\mathbf{x} \sim F_1$, respectively.

Denote $S_1 = 1 - \alpha$, then we can write that:

$$S_1 = \int_{-r}^c \frac{\exp(-x_1^2/2)}{\sqrt{2\pi}} \int_{-\sqrt{r^2-x_1^2}}^{\sqrt{r^2-x_1^2}} \frac{1}{\sqrt{2\pi}} \exp(-x_2^2/2) dx_2 dx_1. \tag{A2}$$

Using the error function, Equation (8) can be simplified to:

$$S_1 = \int_{-r}^c \frac{\exp(-x_1^2/2)}{2\sqrt{2\pi}} \left[\operatorname{erf}\left(\frac{\sqrt{r^2-x_1^2}}{\sqrt{2}}\right) - \operatorname{erf}\left(-\frac{\sqrt{r^2-x_1^2}}{\sqrt{2}}\right) \right] dx_1. \tag{A3}$$

Noting that:

$$\frac{d}{d\alpha} \int_{\phi(\alpha)}^{\psi(\alpha)} f(x, \alpha) dx = \frac{d\psi}{d\alpha} f(\alpha, \psi) - \frac{d\phi}{d\alpha} f(\alpha, \phi) + \int_{\phi(\alpha)}^{\psi(\alpha)} \frac{\partial f}{\partial \alpha} dx,$$

and

$$\frac{d}{dz} \operatorname{erf}(z) = \frac{2}{\sqrt{\pi}} \exp(-z^2),$$

we have that:

$$\frac{dS_1}{dr} = \frac{\exp(-c^2/2)}{2\sqrt{2\pi}} \left[\operatorname{erf}\left(\frac{\sqrt{r^2-c^2}}{2}\right) - \operatorname{erf}\left(-\frac{\sqrt{r^2-c^2}}{\sqrt{2}}\right) \right] \times \frac{dc}{dr} + \int_{-r}^c \frac{\exp(-r^2/2)}{\sqrt{2\pi}\sqrt{\pi}} \frac{r}{\sqrt{(r^2-x_1^2)}/2} dx_1. \tag{A4}$$

Since α is fixed, we will have $dS_1/dr = 0$. Therefore:

$$\frac{dc}{dr} = - \left(\int_{-r}^c \frac{\exp(-r^2/2)}{\sqrt{2\pi}\sqrt{\pi}} \frac{r}{\sqrt{(r^2 - x_1^2)/2}} dx_1 \right) \Big/ \left(\frac{\exp(-c^2/2)}{2\sqrt{2\pi}} \times \left[\operatorname{erf}\left(\frac{\sqrt{r^2 - c^2}}{2}\right) - \operatorname{erf}\left(-\frac{\sqrt{r^2 - c^2}}{2}\right) \right] \right). \quad (A5)$$

Following very similar steps, we have that:

$$\begin{aligned} \frac{d\beta_1}{dr} &= \frac{\exp(-(c - d_1)^2/2)}{2\sqrt{2\pi}} \left[\operatorname{erf}\left(\frac{\sqrt{r^2 - c^2}}{\sqrt{2}}\right) - \operatorname{erf}\left(\frac{-\sqrt{r^2 - c^2}}{\sqrt{2}}\right) \right] \times \frac{dc}{dr} \\ &+ \int_{-r}^c \frac{\exp(-(r^2/2) - (d_1^2/2 - d_1x_1))}{\sqrt{2\pi}\sqrt{\pi}} \frac{r}{\sqrt{(r^2 - x_1^2)/2}} dx_1, \end{aligned} \quad (A6)$$

where

$$\beta_1 = \int_{-r}^c \int_{\sqrt{-r^2 - x_1^2}}^{\sqrt{r^2 - x_1^2}} \frac{1}{2\pi} \exp\left(-\frac{1}{2}((x_1 - d_1)^2 + x_2^2)\right) dx_1 dx_2.$$

Substituting Equation (A5) into Equation (A6) we have:

$$\begin{aligned} \frac{d\beta_1}{dr} &= \frac{\exp(-d_1^2 - r^2/2)}{\sqrt{2\pi}} \int_{-r}^c (\exp(d_1x_1) - \exp(cd_1)) \\ &\times \frac{r}{\sqrt{(r^2 - x_1^2)/2}} dx_1. \end{aligned} \quad (A7)$$

Clearly, since $x_1 < c$ because $x_1 \in [-r, c)$, the integrand in Equation (A7) is always less than zero except for one data point. Hence, we can conclude that $d\beta_1/dr < 0$.

It is straightforward to extend the result into a higher-dimensional case because of the properties of multivariate normal distributions. Without loss of generality, we can assume that μ_1 is located on one axis of the coordinate system. Furthermore, the high-dimensional multivariate normal distribution can be projected onto a plane, denoted as S , that contains the mean locations of both F_0 and F_1 .

The projected marginal two-dimensional distribution is still normal (Johnson and Wichern, 1998). Because the control limit of the univariate projection chart is perpendicular to the direction vector of μ_1 , the control limit of the u_1^{DV} chart on the S plane is a line. Therefore, the multi-dimensional problem is reduced to a two-dimensional case. The same results hold.

Biographies

Shiyu Zhou is an assistant professor in the Department of Industrial and Systems Engineering at the University of Wisconsin–Madison. He got his B.S. and M.S. in Mechanical Engineering at University of Science and Technology of China in 1993 and 1996 respectively, and got his Master in Industrial Engineering and Ph.D. in Mechanical Engineering at the University of Michigan in 2000. Dr. Zhou’s research interests are the in-process quality and productivity improvement methodologies by integrating statistics, system and control theory, and engineering knowledge. The objective is to achieve automatic process monitoring, diagnosis, compensation, and their implementation in various manufacturing processes. His research is sponsored by National Science Foundation, Department of Energy, NIST-ATP, and industries. Dr. Zhou is a member of IIE, INFORMS, ASME, and SME.

Nong Jin is a Ph.D. candidate at Department of Industrial and Systems Engineering at University of Wisconsin–Madison. His research area is in the area of modeling, diagnosis, and control of complex manufacturing processes for quality/productivity improvement.

Jionghua (Judy) Jin received her B.S. and M.S. degree in Mechanical Engineering, both from Southeast University in 1984 and 1987 respectively, and her Ph.D. degree in Industrial and Operations Engineering at the University of Michigan in 1999. Dr. Jin is currently an assistant professor in the Department of Systems and Industrial Engineering at the University of Arizona. Her research focuses on developing a unified methodology for quality and reliability improvement through fusion of statistics with the engineering models. Her research expertise is in the areas of systematic process modeling for variation analysis, automatic feature extraction for monitoring and fault diagnosis, and optimal maintenance decision with the integration of the quality and reliability interaction. Her research is sponsored by National Science Foundation, Air Force Office of Scientific Research, U.S. Department of Transportation, and Global Solar Energy Inc., etc. She was the recipient of the CAREER Award from National Science Foundation in 2002 and the PECASE award in 2004, the Best Paper Award from ASME, Manufacturing Engineering Division in 2000. She is a member of INFORMS, IIE, ASQC, ASME, and SME.

Contributed by the Online Quality Engineering Department